THESIS TITLE

BY

SUN MYUNG PARK

THESIS

Submitted in partial fulfillment of the requirements
for the degree of Master of Science in Nuclear, Plasma, Radiological Engineering
in the Graduate College of the
University of Illinois at Urbana-Champaign, 2020

Urbana, Illinois

I think this might be spelled

Master's Committee:

    Assistant Professor Kathryn D. Huff, Adviser *Advisor?*
    Professor xyz

Abstract

Abstract.

Acknowledgments

Acks.

need to acknowledge your fellowship.

Table of Contents

something is strange about this font.

List of Tables

List of Figures

List of Abbreviations

ARE Aircraft Reactor Experiment.

DMSR Denatured Molten Salt Reactor.

DNP delayed neutron precursor.

EVOL Evaluation and Viability of Liquid Fuel Fast Reactor System.

FP fission product.

GIF Generation IV International Forum.

HALEU high-assay low-enriched uranium.

INL Idaho National Laboratory.

INS incompressible Navier-Stokes.

LEU low-enriched uranium.

LMFBR Liquid Metal Fast Breeder Reactor.

LWR Light Water Reactor.

MA minor actinide.

MCFR Molten Chloride Fast Reactor.

MOOSE Multiphysics Object-Oriented Simulation Environment.

MPM Multi-Physics Modelling.

MSBR Molten Salt Breeder Reactor.

MSFR Molten Salt Fast Reactor.

MSR Molten Salt Reactor.

MSRE Molten Salt Reactor Experiment.

ORNL Oak Ridge National Laboratory.

PDE partial differential equation.

RANS Reynolds-averaged Navier-Stokes.

SAMOFAR Safety Assessment of the Molten Salt Fast Reactor.

TRU transuranic.

Chapter 1

Introduction

1.1 Background and Motivation

Since the Industrial Revolution in the 1800s, rapidly rising greenhouse gas emissions have contributed significantly to global warming. The consequences have been acutely felt in recent years through increasingly frequent and record breaking extreme weather events. Urgent measures are necessary to limit CO_2 emissions and the negative impacts of global warming.

Since electricity generation from burning fossil fuels represents the largest source of CO_2 emissions (38% in 2018 [1]), replacing them with low-carbon alternatives would effectively curb a large fraction of emissions. Out of all low-carbon power sources, nuclear power is arguably best suited to replace fossil fuel burning; it provides consistent base-load power independent of weather and local geographical conditions. Solar and wind power are dependent on favorable weather conditions while hydropower requires relatively more area and is limited to geologically appropriate locations. This argument provides a strong case for nuclear power being the most appropriate and realistic alternative to burning fossil fuels for our current and future electricity needs.

Large-scale reactor deployments are necessary to displace the presently large share of energy production from fossil fuel power plants. However, several obstacles stand in the way of mass reactor deployments. These include perceived safety risks, sustainability concerns, nuclear proliferation risks, and the ability to compete economically with other sources of energy. The Molten Salt Reactor (MSR) concept, one of six advanced reactor designs selected by the Generation IV International Forum (GIF) [2] for continued research and development, is a potential solution to

the aforementioned issues.

The primary coolant in MSRs is a molten salt mixture with fissile and/or fertile material directly dissolved in the coolant. MSRs possess an inherently robust safety feature in the strongly negative fuel temperature reactivity coefficient from Doppler broadening and thermal fuel expansion that greatly reduces the risk of a reactor power excursion. Many designs can also incorporate the thorium fuel cycle for improved sustainability arising from the use of abundant natural thorium resources and reduced transuranic waste. The resultant reduced radiotoxicity from transuranic waste also reduces costs associated with long-term nuclear waste storage. In addition, the ability to operate at near atmospheric pressures eliminates the need for a thick pressure vessel and drives down construction costs, while online fuel reprocessing reduces reactor downtime during reactor operation.

However, the liquid fuel form also brings about novel computational challenges in simulating the transient behavior of MSRs; the neutronics and thermal-hydraulics are more tightly coupled due to the strong temperature reactivity coefficient and the additional advection coupling terms. Furthermore, we have to account for the movement of delayed neutron precursors (DNPs) as they are now generated directly within the primary coolant loop. Therefore, the choice of coupling methods for each set of physics requires careful consideration. Existing reactor system-level codes and modeling approaches for conventional Light Water Reactor (LWR) analysis contain reactor-specific assumptions in multiphysics coupling and other areas that render the techniques less suitable for simulating MSRs. Thus, making minor modifications to these codes without changing the underlying algorithms is not the best approach for MSR safety analysis.

In the past two decades, researchers have developed several new tools for simulating steady-state and transient behavior in MSRs. Many of the earlier efforts featured simplifications in simulating thermal-hydraulics by solving 1-D Navier-Stokes equations or using predetermined uniform velocity fields [3] [4]. In more recent years, there has been significant progress towards fully coupled, spatial codes that feature 2-D axisymmetric or full 3-D models. In 2011, Cammi et al. [5] performed a "Multi-Physics Modelling (MPM)" analysis of a simplified 2-D axisymmetric

2

model of a single Molten Salt Breeder Reactor (MSBR) fuel channel using the commercial finite element analysis software COMSOL Multiphysics. The physics were implemented through the two-group neutron diffusion equations, and the Reynolds-averaged Navier-Stokes (RANS) standard $k - \epsilon$ turbulence model for the neutronics and thermal-hydraulics respectively. The authors emphasized the need for proper full coupling of the multiphysics and presented both steady-state and transient results in various scenarios such as reactivity insertions, changes in pumping rate, and the presence of periodic perturbations. This approach was featured again in a later paper by Fiorina et al. [6] in 2014 for a 2-D axisymmetric model of the Molten Salt Fast Reactor (MSFR). The authors presented results from the Politecnico di Milano COMSOL-based approach and another approach by researchers from Delft University of Technology, in which they coupled their in-house neutronics and thermal-hydraulics codes, DALTON and HEAT respectively. With multigroup neutron diffusion and RANS formulations on ultra fine meshes, both models showed good agreement in the steady-state neutron flux, temperature, and DNP distributions, and in the power responses following various accident transient initiations. Aufiero et al. [7] concurrently developed a full-core 3-D model of the MSFR on OpenFOAM, albeit with one-group neutron diffusion to reduce computational load. With the 3-D model, the authors could simulate the asymmetric reactor response to the failure of a single pump in the sixteen-pump MSFR configuration. The authors also provided some quantitative data supporting the use of implicit coupling over explicit coupling to obtain accurate solutions of the transient cases. Recognizing the huge computational burden required for full 3-D simulations, later authors came up with innovative ways to alleviate this issue such as selective geometrical reduced order modeling for various components of a reactor based on the importance of the physical phenomena being simulated [8], or using a novel, efficient method for neutronics calculations [9].

The preceding discussion highlights the challenges faced in MSR simulation, and the need for a highly efficient simulation tool that incorporates implicitly coupled multiphysics with good computational scalability over multiple processing units. This paper presents the open

3

source MSR simulation tool, Moltres, as a strong contender to overcoming these challenges for simulating the MSFR. Moltres is an application code built in the Multiphysics Object-Oriented Simulation Environment (MOOSE) parallel finite element framework. Similar to COMSOL and OpenFOAM, it solves the deterministic multigroup neutron diffusion and thermal-hydraulics partial differential equations (PDEs) simultaneously on the same mesh. It supports up to 3-D meshes and scales well for a large number of processors.

Moltres employs fully implicit coupling between the neutronics and thermal-hydraulics governing equations, to fully account for the tightly coupled physics expected in MSRs due to the movement of fuel in the salt. We implemented flow using the Navier-Stokes equations and zeroth-order approximation of eddy viscosity for a more accurate representation of the flow profile compared to imposing a predetermined velocity field.

1.2 Objectives

The main objective of this thesis is to demonstrate Moltres' capabilities in modeling multiphysics, steady-state, and transient behavior of fast-spectrum MSRs through the study of the MSFR concept. This is achieved by first verifying Moltres' neutronics results against Serpent in the context of the MSFR, and then comparing the coupled neutronics/thermal-hydraulics steady-state and transient accident results of the MSFR concept. The multiphysics results are verified against the results by Fiorina et al. [6] and Aufiero et al. [7].

1.3 Thesis Outline

The outline of this thesis is as follows: Chapter 2 discusses the history and features of MSRs. The MSFR concept is covered in greater detail. Chapter 3 details the simulation codes and the general modeling approach for generating the results in this thesis. Chapter 4 provides a neutronics assessment by comparing key neutronics parameters from Moltres' eigenvalue

calculations to Serpent's Monte Carlo calculations. Chapter 5 presents steady-state results of coupled neutronics/thermal-hydraulics MSFR simulations in Moltres. Chapters 6 to 9 present transient accident simulation results for unprotected reactivity insertions, unprotected loss of flow, unprotected pump overspeed, and unprotected loss of heat sink, respectively. Lastly, Chapter 10 summarizes the key findings of this thesis and posits some potential avenues for future work.

Way too many chapters! Combine.

Literature review and motivation need to be stronger & clearer.

Why the MSFR? Why Moltres? Why MSRs at all? Why validate anything? Why verify? Why simulate accidents? What is the broad arc of MSRs? Multiphysics? Multiphysics in MSRs (more papers than those cited here are present in the literature.)

Chapter 2

Molten Salt Reactors

MSRs are one of six advanced reactor designs shortlisted by the GIF in 2001 for promising significant advances in safety, sustainability, efficiency, and cost over existing designs in operation today. This has attracted significant attention and resources towards MSR research, most noticeable by the number of start-up companies that have emerged in recent years touting various MSR designs. This chapter provides a brief history of MSRs, followed by the distinctive features that earned the concept the label of being a Generation IV reactor. Lastly, we present the reference specifications of the MSFR concept studied in this work.

2.1 History

The first MSR, named the Aircraft Reactor Experiment (ARE), dates back to the 1940s as part of the US Aircraft Nuclear Propulsion program [10]; the molten salt concept was considered due to the stability of molten salts at high temperatures and neutron radiation. The 2.5 MW_{th} reactor was built at Oak Ridge National Laboratory (ORNL), where it achieved criticality on November 1954 and generated 100 MWh over nine days [10]. The fuel consisted of enriched uranium in a molten salt mixture of NaF, ZrF_4, and UF_4, and was moderated by blocks of beryllium oxide. The project ultimately never came to fruition as the development of intercontinental ballistic missiles effectively eliminated the need for long-range nuclear-powered bomber aircraft.

However, the successful demonstration of the ARE spurred further research into adapting MSRs for civilian power generation [10]. One of the key findings from the research was that breeding ^{233}U from ^{232}Th gave better performance than breeding ^{239}Pu from ^{238}U in thermal-spectrum

reactors. Ultimately, these efforts culminated in the design, construction, and successful operation of the Molten Salt Reactor Experiment (MSRE), a graphite moderated thermal MSR. Although the experiment did not include breeding, scientists at ORNL obtained a wealth of other experimental data and new insights from the study of this reactor. The MSRE had a graphite-moderated design with a LiF-BeF$_2$-ZrF$_4$-UF$_4$ fuel salt mixture, initially rated at 10 MW$_{th}$ but later restricted to 8 MW$_{th}$ due to a miscalculation of heat transfer capabilities [11].

Design of the MSRE commenced in the summer of 1960, with construction starting in early 1962 [11]. The reactor achieved zero-power criticality in June 1965, and 30 days of continuous operation at full power in December 1966. The reactor operated at full power for the most of the following 15 months, during which the researchers carried out various experiments. Soon after shutdown, the ^{235}U fuel was replaced with ^{233}U and in January 1969, the MSRE became the first reactor to run on ^{233}U fuel. Further experiments were run, including xenon stripping, fission product deposition, tritium behavior, and plutonium addition studies, before the MSRE was permanently shut down to conserve remaining funding for other related activities [12].

Building on the MSRE's hugely successful run, ORNL proposed a new program for the construction and operation of a demonstration reactor based on the MSBR concept that they had developed [12]. The MSBR is a thermal-spectrum, single fluid reactor with fertile ^{232}Th isotopes mixed directly into the FLiBe molten salt for ^{233}U breeding [13]. Like the MSRE, the MSBR relies on continuous online reprocessing to add fertile material and remove fission product (FP) neutron poisons. As a breeder reactor, the doubling time (the minimum amount of time required to produce enough fissile material to start up another MSBR) was estimated to be approximately 22 years. However, ORNL failed to secure funding on two separate occasions in 1972 and 1974; they lost out to the competing Liquid Metal Fast Breeder Reactor (LMFBR) program which had a head start and wider political and technical support. Nevertheless, from a technical perspective, two independent technology evaluation and design studies of the MSR had "reported favorably on the promise of the system" [12].

In spite of this setback, research into MSRs continued through the late 1970s. In 1980, ORNL

published a report describing a new MSR concept, called the Denatured Molten Salt Reactor (DMSR) [13]. This design was developed in response to the fuel reprocessing restrictions introduced by President Ford in 1976; the DMSR is designed to operate as a once-through converter system without fuel reprocessing. While it is largely fueled by 19.75 % high-assay low-enriched uranium (HALEU), the initial core loading includes thorium to boost its conversion ratio throughout its lifetime. It has a continuous online feed consisting of HALEU to maintain criticality, and denatured ^{235}U to keep uranium enrichment levels below nuclear non-proliferation policy thresholds. The design also includes a gas sparging system for removing gaseous FPs, while noble metals naturally plate out onto the walls of the coolant loop. A significant drawback in the MSBR design is the extensive neutron damage in the graphite moderator that necessitated frequent replacement (every four years) throughout its operational lifetime. The DMSR avoids this issue by having a lower power density while maintaining the overall power output of 2250 MW$_{th}$. As a result, the graphite moderator was projected to last for the entirety of the DMSR's design lifetime.

There was a concurrent program at the UK Atomic Energy Authority for the development of a 2500 MW$_e$ lead-cooled Molten Chloride Fast Reactor (MCFR) concept [14]. It is a dual fluid system, with separate loops for the fuel salt and the blanket salt. The blanket is a 1 m-wide tank surrounding the core. The relatively harder neutron spectrum arising from the absence of moderators and the choice of chloride over fluoride salt favors ^{239}Pu breeding over the thorium cycle. Some experiments were performed to study molten salt chemistry but no reactor prototypes were built. The UK program was eventually shut down just like its US counterpart partly due to the successful demonstration of the Prototype Fast Reactor which had achieved criticality in 1974.

Following a lull lasting through the late 20th century, MSR research picked up pace due to renewed interest initiated by the GIF in 2001. Today, there are numerous MSR concepts under active development led by various national and commercial bodies. Many differences exist between different concepts and the only common denominator is the use of nuclear fuel

dissolved in molten salt.

2.2 Features

As mentioned in the introduction section, the most significant difference between MSRs and other reactor concepts is the liquid fuel in MSRs; fissile and/or fertile material is dissolved in high temperature, commonly eutectic mixtures of molten salts. Most MSR designs are circulating-fuel reactors. The primary coolant loop containing the fuel salt transfers heat through a heat exchanger to the clean, secondary/intermediate loop. The liquid fuel form allows for continuous online fuel reprocessing, and the removal of gaseous FPs via a gas sparging system.

The flexibility of MSRs is best illustrated by the various designs under development today. Graphite-moderated thermal-spectrum MSRs are typically straightforward low-enriched uranium (LEU) burners or ^{232}Th/^{233}U iso-breeders/breeders, while epithermal- and fast-spectrum MSRs have the additional options of operating as transuranic (TRU) fuel burners or ^{238}U/^{239}Pu breeders. Breeder designs can be further categorized into one- or two-fluid designs; two-fluid designs feature separate blanket molten salt mixtures that contain higher proportions of fertile material than the fuel salt mixture.

2.2.1 Safety

MSRs are generally deemed to be safer than LWRs due to their reliance on natural physical phenomena for passive safety. The most immediate and significant safety characteristic is the strong negative temperature reactivity feedback of the fuel salt. This is due to greater temperature-induced volumetric expansion in liquid fuel than solid fuel. Combined with the Doppler broadening of resonance capture cross sections present in both fuel forms, we expect to observe a smaller temperature increase following an unprotected reactivity insertion. The overall temperature reactivity coefficient varies widely between different MSR designs due to other structures, such as moderators and reflectors, present in the core. In particular, graphite

9

moderators tend to have slightly positive temperature reactivity coefficients. This was notably observed in the MSBR concept, but the total temperature reactivity coefficient was still relatively large and negative [15]. This phenomenon provides a large degree of control and stability as it is always present in an MSR regardless of the operating conditions.

Continuous online fuel reprocessing allows operators to maintain low excess reactivity inventories in the core as additional fuel can be added on an ad hoc basis. Reprocessing and gas sparging systems help reduce fissile requirements by continuously removing neutron poisons. These factors, in addition to the strong negative temperature reactivity coefficient, diminishes the likelihood and severity of unprotected criticality accidents in MSRs [16]. In the unlikely situation where an MSR encounters a severe runaway reaction, we can rely on another passive safety feature: freeze plugs. A freeze plug is a plug of solidified salt at the bottom of the core actively cooled by fans or other cooling systems to keep its temperature just below the freezing point of the salt [17]. When temperatures in the core exceed a certain threshold during a dangerous transient, the freeze plug melts and the molten salt in the core drains into a containment tank designed to keep the salt in a subcritical configuration. This is especially easy to achieve for thermal-spectrum MSRs as the absence of moderators in the containment tank would automatically bring the multiplication factor down below unity [16]. MSRs also typically have large margin-to-boiling under nominal operating conditions so that fuel salt boiling does not occur. Furthermore, the reactor vessel is consequently subject to much lower stresses as MSRs operate at near-atmospheric pressure levels. Thus, the probability of pipe ruptures due to high pressure is low.

MSRs may be more resilient to pump failure accidents as natural circulation could passively sustain enough heat transfer through the heat exchanger to remove any remaining fission and decay heat after the failure. If natural circulation proves insufficient, the aforementioned freeze plug can drain the salt out of the core. Decay heat in MSRs with online reprocessing is typically lower than that in LWRs due to the continuous removal of FPs. For example, the decay heat in an MSFR after reaching equilibrium salt composition is expected to be approximately 3.5% of full

reactor power compared to 6% in LWRs [18].

However, there are also some safety disadvantages associated with MSRs. Firstly, MSRs have smaller fractions of DNPs in the active core region as some of them decay in the external loop regions; this complicates reactor control and may result in faster transients due to the decrease in average neutron lifetime. Secondly, structural materials in the core must be resistant to salt corrosion under high temperatures and neutron irradiation over the lifetime of the reactor. To a lesser extent, pipes should also be corrosion resistant to prevent pipe ruptures. Lastly, fuel salt overcooling is a potentially dangerous accident scenario as the strong temperature coefficient can effectively cause a large reactivity insertion. Overcooling may also cause salt to freeze and restrict flow, thereby causing a complete loss of flow accident.

2.2.2 Other Factors

Other factors for assessing a reactor design include sustainability, economics, waste management, and non-proliferation.

Breeder MSR designs easily score well in the sustainability category. MSRs generally have good neutron economy due to little structural material in the core and continuous online removal of neutron poisons. Noble metal neutron poisons also naturally plate out onto the inner walls of the loop which are generally regions of lower neutronic importance. Both ^{232}Th/^{233}U and ^{238}U/^{239}Pu fuel cycles are viable candidates for breeding in MSRs, with the former being more suited for thermal reactors and the latter being more suited for fast reactors. Another benefit of this is that some MSRs can potentially start with an initial core loading of ^{239}Pu with a fast spectrum before transitioning towards ^{233}U fuel with a ^{232}Th feed; this measure effectively circumvents the issue of having insufficient ^{233}U inventory to start up the reactor.

The ^{232}Th/^{233}U fuel cycle produces significantly less TRU waste than the other cycles due to the smaller atomic masses of ^{232}Th and ^{233}U. This reduces the overall radiotoxicity and long-term decay heat associated with long-lived plutonium and minor actinide (MA) isotopes. However, there are other radionuclides such as ^{231}Pa, ^{229}Th, and ^{230}U that may pose long-term radiological

I thought TRU burning was the feature under discussion..

concerns. Nevertheless, this feature complements TRU burning in fast spectrum MSRs to reduce overall levels of TRU waste going into long-term storage in nuclear waste repositories.

There are some nuclear non-proliferation concerns with the *in thorium-fueled* thorium fuel cycle in MSRs. The main concern involves the separation of the intermediate ^{233}Pa isotope from the fuel salt. ^{233}Pa decays into ^{233}U with a half-life of approximately 27 days and ^{233}U is at least as potent as ^{235}U for nuclear weapons production. The highly radioactive ^{232}U provides some level of proliferation resistance but it can be sidestepped by separating away its ^{232}Pa precursor, which has a half-life of only 1.31 days. Strong regulatory framework and close monitoring of MSRs would be essential *are therefore* to ensure non-proliferation.

Safeguards by design
avoiding SNM diversion.
cite the SQ
[Citations & literature review regarding MSR safeguards would be appropriate here.]

The economic prospects are uncertain at the current stage of MSR development but we can qualitatively list the potential impacts. Capital costs are expected to be greater due to the need for increased corrosion resistance and the supporting reprocessing facilities. This is in spite of the reduced pressure constraints on the reactor pressure vessel for MSRs resulting from the *constraints* *due to* significantly lower operating pressure. There are potential cost savings from eliminating fuel pellet and fuel assembly fabrication. Higher fuel utilization is achievable as neutron poisons are continuously removed from the core via the continuous online reprocessing and gas sparging systems. Online fuel reprocessing also minimizes reactor downtime because refuelling can be performed at any time. The higher operating temperature results in greater thermal efficiencies and presents new opportunities beyond conventional electricity generation, namely industrial process heat applications and hydrogen production.

This should be replaced by a review of the literature regarding MSR economics.

Beyond these factors, MSRs still require significant R&D efforts and engineering demonstrations for experimental validation of various components before a full commercial model can be commissioned. Work towards creating a safety and licensing framework for MSRs has picked up pace only in recent years due to the growing interest from commercial MSR developers.

2.3 Molten Salt Fast Reactor

The MSFR is a reference fast-spectrum MSR concept developed under the Evaluation and Viability of Liquid Fuel Fast Reactor System (EVOL) and Safety Assessment of the Molten Salt Fast Reactor (SAMOFAR) projects. The main reactor specifications and schematic view are shown in Table 2.1 and Figure 2.1, respectively. Developed from the MSBR, the MSFR is intended to run primarily on a closed thorium fuel cycle with continuous online fuel reprocessing. Several reasons motivated the omission of graphite moderators from the MSFR design. Graphite is susceptible to long-term radiation damage and replacement is likely to be necessary during the operating lifetime of the reactor. Graphite also has a positive temperature coefficient of reactivity; eliminating graphite from the design ensures a greater safety margin [19]. While negative temperature coefficients are attainable with very thermalized spectra, breeding ratios deteriorated significantly due to parasitic absorption in the large volume of graphite needed for thermalization [19].
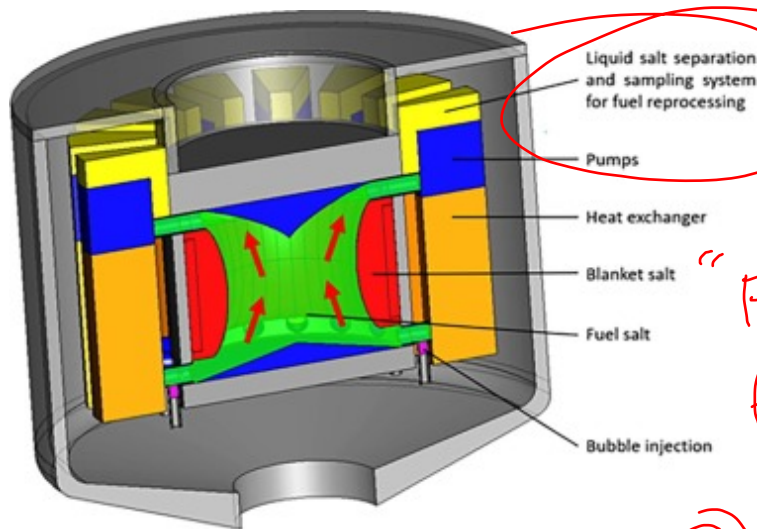
Figure 2.1: Schematic view of the MSFR concept [20].

In the MSFR design, fuel salt flows upwards through a 9 m^3 central core region. At the top of the core, the flow separates into sixteen smaller external loops, each of which passes through a heat exchanger before being pumped back into the bottom of the core. Other instrumentation

13

Table 2.1: Main specifications of the MSFR concept [20].

Parameter	Value
Thermal/Electric output [MW_{th}/MW_e]	3000 / 1500
Salt volume [m^3]	18
Salt fraction in core	0.5
Number of circulation loops	16
Nominal flow rate [$kg\,s^{-1}$]	18500
Nominal circulation time [s]	4.0
Inlet/outlet temperature [K]	923 / 1023
Blanket volume [m^3]	7.3

are situated along the external loop for online salt reprocessing and gas sparging. The core is surrounded axially by nickel alloy reflectors, and radially by a toroidal blanket tank containing fertile salt for breeding. There is a layer of boron carbide behind the blanket tanks to protect the peripheral equipment from excessive neutron damage. In case of severe accidents, there is an actively cooled freeze plug at the bottom of the core that melts when temperatures exceed a certain threshold. The fuel salt would drain into a containment vessel designed to keep it subcritical. Reactivity control under normal operating conditions is performed by varying pump speeds to take advantage of the strong thermal feedback. Coupled with the fact that there is no excess reactivity reserve due to online fuel reprocessing, there are no control rods in the MSFR design.

Although the MSFR is primarily designed to operate on the thorium fuel cycle, it can support a range of start-up fuel and feed compositions. This versatility is particularly important for the first few MSFRs to be deployed due to the lack of ^{233}U reserves required for the initial core loading. In general, the fuel and blanket salts are approximately composed of eutectic mixtures of 77.5% LiF - 22.5% AcF_4, where AcF_4 represents actinide fluorides such as uranium, thorium, plutonium, and other TRU fluorides. For an initial composition consisting of ^{232}Th and ^{233}U, the benchmark value for the amount of uranium for criticality under normal operating conditions is 2.515 mol%. However, most code verification studies adjust the ratio of ^{232}Th to ^{233}U to achieve exact criticality at a uniform temperature of 973 K; this ensures that subsequent neutronics and safety analyses are not affected by the difference in k_{eff} values. We performed the same exercise

14

in this thesis.

Power output of the MSFR is rated at 3000 MW$_{th}$ and 1500 MW$_e$. It has a high thermal efficiency due to the high operating temperature. MSRs in general are not restricted by the same pressure constraints seen in LWRs. The inlet and outlet temperature specifications of the fuel salt are 923 K and 1023 K, respectively. This was motivated by the need for a minimum 50 K temperature buffer between the operating temperatures and the melting point of the salt. The MSFR has heat exchangers and an intermediate coolant loop to isolate the power conversion system from the highly radioactive fuel salt. This also serves as a layer of containment between the radioactive material and the outside environment. The exact composition of the intermediate coolant is still under active study and not finalized yet.

2.3.1 Model Geometry

For this work, we used a model similar to the reference square-cylindrical MSFR design to benchmark our results against results published by Fiorina et al. and Aufiero et al. The reference design is a 2-D axisymmetric model with the sixteen individual external loops homogenized into a single outer loop as shown in Figure 2.2. For the multigroup cross sections and group constants calculations in Serpent, we extended this 2-D axisymmetric model into a 3-D model by a simple full rotation about the central axis. The material definitions are the same as those specified in the reference MSFR model. Accordingly, the pump and heat exchanger regions are assumed to be composed of 100% fuel salt. While this may not be entirely accurate, the exact details of the pump and heat exchanger systems are still under active study, and this external loop region is presumed to be of little neutronic importance due to its position behind the strong boron carbide neutron absorber layer.

Although we used the exact reference model for generating group constant data from Serpent, there are two minor differences between the MSFR model geometry we used in Moltres, and the Polimi/TUDelft models. The first difference is a relative minor change to the mesh by the exclusion of the 2 cm thick structural material around the blanket tank that separates the

15
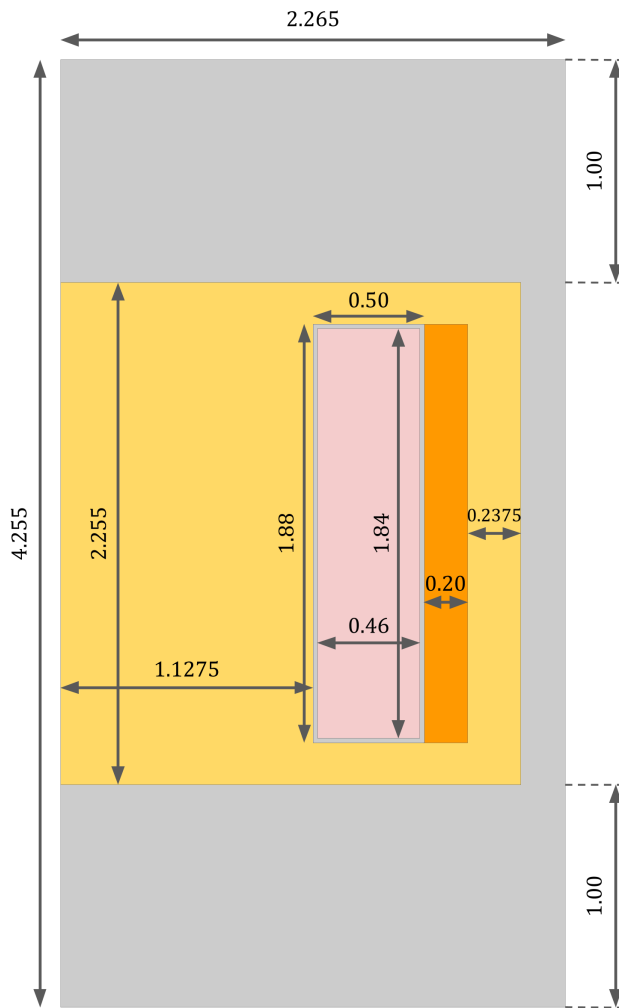
Figure 2.2: 2-D axisymmetric model of the MSFR core used for the simulations in Serpent. All dimensions are in meters. [21]

fuel and blanket salts. We removed this feature in our finite element mesh as we encountered difficulty meshing this layer that is relatively much thinner than the rest of the model. Any impact on the neutron flux is expected to be minimal. Furthermore, we solved for the temperature distribution only in the primary loop and applied homogeneous Neumann boundary conditions for temperature on the core walls, as was done in the Polimi/TUDelft models. Therefore, we believe the overall impact on the results is negligible.

The second difference pertains to the modeling of the external loop. In its current implementation, Moltres lacks sophisticated pump- and heat exchanger-equivalents in the code. Thus,

16

the external loop, beyond the central region of the primary loop where most of the fissions take place, is modeled as a 1-D pipe with a simple, point heat sink to represent the heat exchanger. Instead of pumps, a Dirichlet boundary condition for velocity at the inlet boundaries drives the flow in the central core region of the primary loop. All flow-dependent variables such as temperature, DNPs, and decay heat precursors are fully conserved as they loop around between the two regions. As a result, this approach shares some similarities with the geometric multiscale modeling approach by Zanetti et al. [8]. Future models could create a better representation of the primary loop by implementing a whole continuous loop with pressure increases and drops corresponding to the pumps and heat exchangers.

2.3.2 Material Specifications

This section details the material specifications of the various reactor components in the MSFR.

Molten Salt

As mentioned before, the fuel and blanket salts are comprised of a 77.5% LiF - 22.5% AcF_4 mixture. This is the reference salt composition of the MSFR at start-up. Typically, researchers working with the MSFR model calculate the exact actinide composition by varying the ^{232}Th to ^{233}U ratio to obtain a k_{eff} value of 1 at a uniform temperature of 973 K. Thus, the exact actinide compositions vary depending on the nuclear data library and neutron transport code. The exact composition used for this work can be found in the Results chapter. We assume that the effects of these composition variations on the reference physical properties of the fuel and blanket salt are negligible. Table 2.2 shows relevant physical properties of the fuel and blanket salts.

Structural Materials

The reflectors on the periphery of the reactor core and the blanket tank are made of a nickel-based alloy provided from reference specifications [22]. Table 2.3 details the compositions of the nickel-based alloy and boron carbide absorber. The alloy has a density of 10 g cm^{-3}. The

17

Table 2.2: Properties of the fuel and blanket salts LiF-AcF$_4$.

Property	Formula	Value at 973 K	Validity Range
Melting temperature [K]	841	N/A	1 bar
Boiling temperature [K]	1874	N/A	1 bar
Density, ρ [kg m^{-3}]	$4094 - 0.882 \cdot (T - 1008)$	4125	893-1123 K
Dynamic viscosity, μ [Pa s]	$\rho \cdot 5.55 \times 10^{-8} \cdot e^{3689/T}$	1.015	898-1121 K
Thermal conductivity, k [W m^{-1} K^{-1}]	$0.928 + 8.397 \times 10^{-5} \cdot T$	0.01010	891-1020 K
Specific heat, c_p [J kg^{-1} K^{-1}]	$-1111 + 2.78 \cdot T$	1594	867-907 K

material composition of the reflectors may be subject to minor changes, but it is not a major

concern as the reflectors are not situated in regions of high neutron flux. The MSFR also includes

a 20 cm layer of boron carbide (B$_4$C) to protect the heat exchangers and pumps from neutron

irradiation. The reference specifications indicate that natural boron is used, which is composed

of 19.8 % ^{10}B and 80.2 % ^{11}B, with an overall density of 2.52 g cm^{-3}.

Table 2.3: Composition (mol %) of the nickel-based alloy used in the simulation of the MSFR in
this work.

Ni	W	Cr	Mo	Fe	Ti	C	Mn	Si	Al	B	P	S
79.432	9.976	8.014	0.736	0.632	0.295	0.294	0.257	0.252	0.052	0.033	0.023	0.004

Chapter 3

Modeling Approach

[handwritten: This work demonstrates the MSFR simulation capabilities of Moltres, a multiphysics .....]

[handwritten: sounds like the beginning of an apology?]

The main simulation tool used in this work for studying the MSFR is Moltres. While we used Moltres for the steady-state and transient analysis, it requires a dedicated neutron transport solver such as Serpent 2 to generate neutron energy group constant data for the multigroup neutron diffusion calculations in Moltres. This chapter provides brief introductions of the Serpent and Moltres codes, and the general modeling approach for the multiphysics simulations in Moltres.

[handwritten: dedicated implies some kind of coupling.]

[handwritten: Please cite these tools.]

[handwritten: Please review the writing checklis]

3.1   Serpent 2

Serpent 2 [23] is a continuous-energy Monte Carlo reactor physics code under active development at the VTT Technical Research Centre of Finland. It was created in 2004 out of the need for better general-purpose neutron-transport codes for group constant generation in lattice geometries, and has since grown to support more general capabilities, for an active user base of more than 500 people worldwide. Serpent is highly parallelizable, due to its support for both MPI and OpenMP parallel programming APIs, and highly validated and verified against experimental data and other well-established codes.

[handwritten: neutron transport application]

[handwritten: led by]

[handwritten: better how? (C++)]

[handwritten: citation needed]

[handwritten: supporting]

[handwritten: It has also been cite the validation & verification articles]

In Serpent, each neutron is tracked through a combination of ray-tracing-based surface tracking and rejection sampling-based delta-tracking. Users may define the number of neutron histories and the number of active and inactive cycles for each simulation. Inactive cycles are required for fission source distribution convergence, before interactions are tallied in the active cycles. Interaction types and locations are determined stochastically based on neutron interaction data

[handwritten: histories]

from established nuclear data libraries (e.g. ENDF, JEFF). These nuclear data libraries provide continuous-energy cross section data at discrete temperatures. For other temperatures, Serpent has a built-in Doppler-broadening preprocessor that extrapolates the relevant cross section data from a lower temperature.

In the context of this project, we used Serpent with the JEFF-3.1.2 nuclear data library [24] to generate group constants for Moltres. The reactor geometry is based on the axisymmetric MSFR neutronics benchmark geometry published in several previous papers involving the MSFR, as shown in Fig. 2.2. The relevant group constant data are collapsed into six neutron energy groups, and calculated for temperature values of 800 K to 1300 K at 50 K intervals.

The group constants relevant for neutronics calculations in Moltres are the macroscopic fission, absorption, and scattering neutron cross sections, neutron diffusion coefficients, average fission energies, average neutron yields, inverse neutron speeds, flux spectra, DNP decay constants, and effective delayed neutron fractions. These group constants are extracted from the Serpent output files using a Python script available from the Github repository that holds the Moltres source code. The script rewrites the group constants into a Moltres-compatible format.

3.2 Moltres

Moltres is a Multiphysics Object-Oriented Simulation Environment (MOOSE)-based application for coupled neutronics/thermal-hydraulics simulations of MSRs. MOOSE [25] is a highly parallelizable, finite element framework developed at Idaho National Laboratory (INL) for simplifying the process of creating fully-coupled, non-linear, multiphysics solvers. The framework provides a user-friendly interface for this task through object-oriented programming in C++. All aspects of a typical multiphysics problem, such as the terms in the PDEs, the initial and boundary conditions, the material properties, etc., are represented in MOOSE as C++ objects. New objects can inherit properties from related old objects to simplify implementation and reduce code duplication. Overall, this approach is helpful for many researchers, a significant fraction of

whom do not possess high-level programming backgrounds, as they are unencumbered by the technical details and complexities involved in programing mesh handling and PDE solving in finite element analysis.

MOOSE itself relies heavily on libMesh [26] and PETSc [27] for its mesh handling and PDE solver functionalities. As a result, MOOSE supports adaptive meshing schemes and automatic variable scaling amongst other advanced features for improved accuracy and performance times. Full coupling is maintained by the execution of Newton-based solves on the weak formulations of the multiple PDEs to minimize the residual values. Fully-coupled solves are essential for accurately resolving systems with strongly interacting physics. The MSR concept is one such example, where the neutronics and thermal-hydraulics are tightly coupled through the Doppler effect and the temperature dependence of liquid fuel salt density.

MOOSE, and Moltres by extension, are capable of up to 3-D geometry modelling. They support a wide range of input mesh file formats listed in a MOOSE webpage, including the commonly used Exodus II file format. Specifically for the 2-D case, axial symmetry is easily and automatically imposed by changing one line of code in the input file, without any changes in the Cartesian representations of the PDEs and boundary conditions in their original C++ implementations. This feature provides significant computational time savings for 3-D systems that exhibit high axial symmetry. Another important feature for reducing computational time is the use of MPI for parallel computing. All MOOSE-based codes can be compiled and run on high performance computing clusters.

As mentioned in the previous chapter, we divided the fuel salt loop into two regions, the central core region where most of the fissions take place, and the outer loop region where the heat exchanger is located. The central core region specifically refers to the central region indicated by the red box in Figure 3.1. We simplified the outer loop into a 1-D pipe as it is a subcritical region and its main purposes are: to introduce a out-of-core residence time for the DNPs, and to site the heat exchanger-equivalent object in Moltres. Accordingly, this section provides separate descriptions for the governing equations in the central core region and the outer loop region.

21
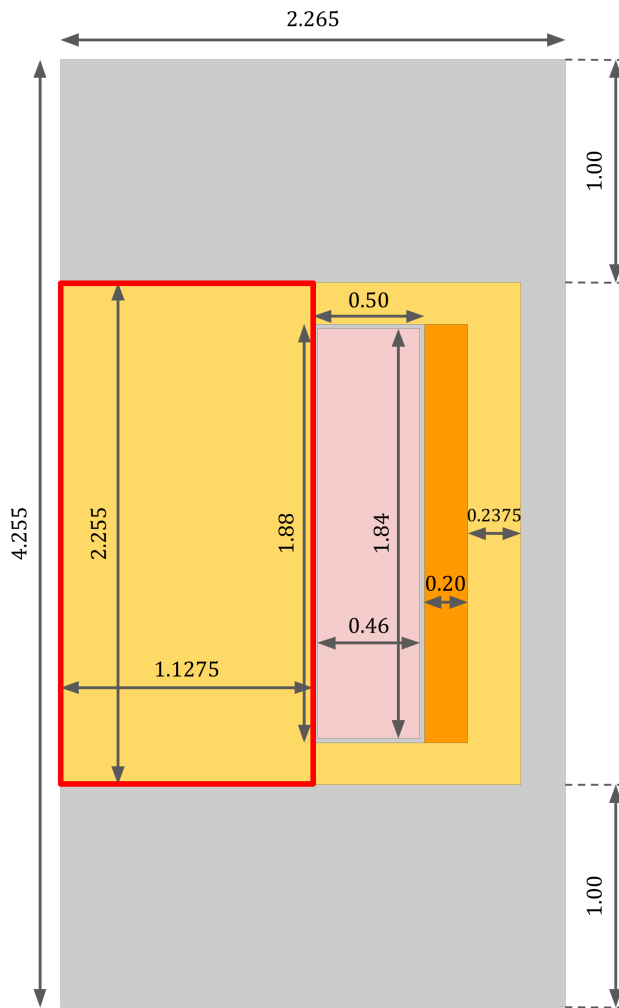
Figure 3.1: 2-D axisymmetric model of the MSFR. The red box indicates the central core region relevant to the modeling approach in Moltres.

There is also a third region ~~comprising~~ Comprised of the blanket salt, the Ni-alloy reflectors, and other material . This region is important for capturing ~~an~~ a more accurate estimate of neutron leakage ~~as opposed to simpler approximations such as~~ imposing fixed albedo boundary conditions on the neutron flux ~~on the neutron fluxes.~~ than would

3.2.1 Central Core Region

The central core region is of greatest interest to us during steady state and transient scenarios; the center of the reactor is naturally where most of the fissions and heat generation occur. Consequently, the PDEs solved for in this region are in their most complete form relatively to simplifying assumptions found in the other regions.

Neutronics Model

The neutron flux calculations in the central core region are performed using the standard formulations for the time-dependent multigroup neutron diffusion equations and DNP concentration equations as shown in equations 3.1 and 3.2:

$$\frac{1}{v_g}\frac{\partial \phi_g}{\partial t} = \nabla \cdot D_g \nabla \phi_g - \Sigma_g^r \phi_g + \sum_{g' \neq g}^{G} \Sigma_{g' \to g}^s \phi_{g'} + \chi_g^p \sum_{g'=1}^{G}(1-\beta)\nu\Sigma_{g'}^f \phi_{g'} + \chi_g^d \sum_i^I \lambda_i C_i, \tag{3.1}$$

$$\frac{\partial C_i}{\partial t} = \beta_i \sum_{g'=1}^{G} \nu\Sigma_{g'}^f \phi_{g'} - \lambda_i C_i - \boldsymbol{u} \cdot \nabla C_i + \nabla \cdot D_t \nabla C_i, \tag{3.2}$$

where

v_g = average speed of neutrons in group g [cm s^{-1}],

ϕ_g = neutron flux in group g [cm^{-2} s^{-1}],

t = time [s],

D_g = diffusion coefficient of neutrons in group g [cm^2 s^{-1}],

Σ_g^r = macroscopic cross section for removal of neutrons from group g [cm^{-1}],

$\Sigma_{g' \to g}^s$ = macroscopic cross section of scattering from g' to g [cm^{-1}],

χ_g^p = prompt fission spectrum for neutrons in group g,

G = total number of discrete neutron groups,

ν = average number of neutrons produced per fission,

23

Σ_g^f = macroscopic fission cross section for neutron in group g [cm^{-1}],

χ_g^d = delayed fission spectrum for neutrons in group g,

I = total number of delayed neutron precursor groups,

β = total delayed neutron fraction,

β_i = delayed neutron fraction of precursor group i,

λ_i = average decay constant of delayed neutron precursors in precursor group i [s^{-1}],

C_i = concentration of delayed neutron precursors in precursor group i [cm^{-3}],

D_t = turbulent diffusion of the delayed neutron precursors [cm^2 s^{-1}].

While the limitations of the multigroup neutron diffusion compared to other deterministic and Monte Carlo methods, particularly for flux values near boundaries, are well-documented, the diffusion model provides acceptable accuracy at lower computational costs. Moreover, the central core region contains no material interfaces except at its boundaries. The ~~Neutronics results section~~ provides a comparison of the MSFR multiplication factor values and reactivity coefficients between Moltres and Serpent.

The DNP concentration equation has additional advection and turbulent diffusion terms to account for the movement of DNPs in the primary coolant loop. The turbulent diffusion value is governed by the following equation:

$$D_t = \frac{\mu_t}{\rho Sc_t} \tag{3.3}$$

where

$$\mu_t = \text{ eddy viscosity [Pa s]},$$
$$\rho = \text{ density of the fuel salt [kg m}^{-3}],$$
$$Sc_t = \text{ turbulent Schmidt number.}$$

We assumed $Sc_t = 0.85$ for a fair comparison with the Polimi/TUDelft models which used the same value.
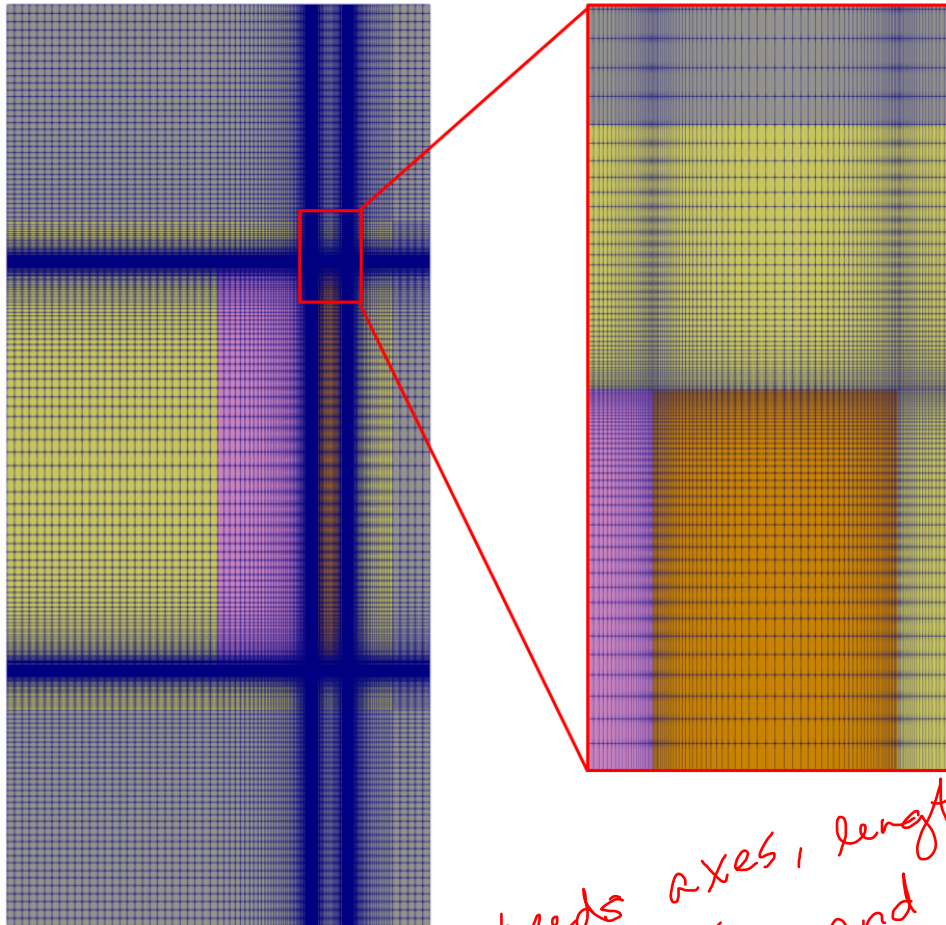
Figure 3.2: Mesh adopted in Moltres and a close-up view of the mesh around the boron carbide absorber.

Moltres users may vary the total number of neutron energy groups as long as they provide Moltres with the appropriate group constant data. The number of precursor groups is also variable, though usually predetermined by the choice of nuclear data library in the group constant generation step. Moltres automatically interpolates the group constant data for required temperatures using one of the many predefined interpolation methods available in MOOSE. Once again, ~~users have the freedom~~ *Moltres allows users* to select their interpolation method of choice.

For this work, we have six neutron energy groups according to the energy boundaries in

Table 3.1: Neutron energy group upper bounds used in Serpent.

Group number	Upper bound [MeV]
1	20
2	2.2313
3	0.4979
4	0.0247875
5	0.0055308
6	0.0007485

table 3.1, eight DNP groups as defined by the JEFF-3.1.2 library, and the spline interpolation method. The neutron flux and DNP concentration values were approximated by first-order Lagrange and constant monomial shape functions respectively on the finite element mesh. Figure 3.2 shows the mesh adopted for the MSFR model. We assumed vacuum boundary conditions for all six neutron group fluxes along the external boundaries of the geometry, and homogeneous Neumann boundary conditions along the axial symmetry boundary. For the DNP concentrations, we imposed homogeneous Neumann boundary conditions on the walls, and inflow and outflow boundary conditions on the inlet and outlet boundaries respectively. The inlet DNP concentration values were imported from the outlet values of the 1-D outer loop pipe at the same timestep.

For the decay heat model, a previous study on the MSFR by Aufiero et al. [28] had shown that using three decay heat precursor groups with different half-lives in the form of exponential equations, can accurately model decay heat in the MSFR for up to 300 seconds after shutdown with a relative error of less than 2%. Thus, we implemented a decay heat model using the following equation:

$$\frac{\partial \omega_k}{\partial t} = f_k \sum_{g=1}^{G} \epsilon_g \Sigma_g^f \phi_g - \lambda^k \omega_k - \boldsymbol{u} \cdot \nabla \omega_k + \nabla \cdot D_t \nabla \omega_k, \tag{3.4}$$

26

where

ω_k = total decay heat power density from decay heat precursors in group k [W cm^{-3}]

f_k = fraction of decay heat to total power at steady state

ϵ_g = average fission energy per fission [W]

λ^k = average decay constant of decay heat precursors in group k [s^{-1}].

Like the neutron and DNP groups, Moltres can take an arbitrary number of decay heat groups. In this work, as with the other parameters, we used the same decay heat fractions and decay constants, shown in Table 3.4, used in the Polimi/TUDelft models for three decay heat groups.

Table 3.2: Decay heat group parameters [6]. λ_i and f_i are the decay constants and decay heat fractions associated to group i.

Decay heat group	λ_i [s^{-1}]	f_i
1	0.1974	0.0117
2	0.0168	0.0129
3	0.000358	0.0186

Thermal-Hydraulics Model

Fluid dynamics in Moltres can be modeled using the incompressible Navier-Stokes (INS) equations with the Boussinesq hypothesis for eddy viscosity. Most of the Navier-Stokes capabilities in Moltres is derived from the MOOSE Navier-Stokes module [29]. The standard INS equations are:

$$\text{Momentum eq.:} \qquad \rho\frac{\partial \boldsymbol{u}}{\partial t} = -\rho(\boldsymbol{u}\cdot\nabla)\boldsymbol{u} + \nabla\cdot(-p\boldsymbol{I} + \mu[\nabla\boldsymbol{u} + (\nabla\boldsymbol{u})^T] + \boldsymbol{f} \tag{3.5}$$

$$\text{Divergence-free:} \qquad \nabla\cdot\boldsymbol{u} = 0 \tag{3.6}$$

27

where

p = pressure [Pa],

μ = dynamic viscosity [Pa s],

$\boldsymbol{f}$ = body force per unit volume [N m^{-3}].

In addition to the intrinsic molecular viscosity, we introduced an eddy viscosity term to approximate turbulent flow effects. The current implementation of Moltres does not have a turbulence model such as the RANS models used in the Polimi/TUDelft models. Thus, we made a zeroth-order approximation of the eddy viscosity based on the results reported in the Polimi/TUDelft models. The eddy viscosity is assumed to be 40 Pa s. Despite the simplicity of this assumption, we were able to reproduce much of the flow profile observed in the Polimi/TUDelft models at steady state.

The energy balance equation for temperature is given in Eq. 3.7. The diffusion term includes turbulent heat diffusivity based on the eddy viscosity μ_t and the turbulent Prandtl number Pr_t, which we assume to be equal to 0.85.

$$\rho c_p \frac{\partial T}{\partial t} = -\rho c_p \boldsymbol{u} \cdot \nabla T + \nabla \cdot [(k + k_t)\nabla T] + Q_s \tag{3.7}$$

$$k_t = \frac{\mu_t}{\rho Pr_t} \tag{3.8}$$

$$Q_s = \left(1 - \sum_{k=1}^{K} f_k\right) \sum_{g=1}^{G} \epsilon_g \Sigma_g^f \phi_g + \sum_{k=1}^{K} \omega_k, \tag{3.9}$$

where

c_p = specific heat capacity of molten salt [J kg^{-1} K^{-1}],

T = temperature of molten salt [K]

$\boldsymbol{u}$ = velocity of molten salt [m s^{-1}],

$$k = \text{thermal conductivity of molten salt } [\text{W m}^{-1}\,\text{K}^{-1}],$$

$$K = \text{total number of decay heat groups.}$$

The first term in the heat source Q_s represents prompt fission heat, and the second term represents decay heat from the K decay heat groups.

We expect good qualitative agreement with the Polimi/TUDelft models, including the large recirculation region near the blanket tank walls and the resulting high temperatures in that region. There would be some minor discrepancies where the viscosity values are under- or over-predicted, leading to slightly inaccurate temperature and precursor concentration values from turbulent diffusion.

3.2.2 Outer Loop Region

Moltres also accounts for the decay of DNPs outside the central core region by simulating its flow in a separate 1-D pipe geometry. This outer loop pipe simulation is implicitly coupled to the active core simulation through Picard iterations in MOOSE's MultiApp functionality and inlet/outlet boundary values. For this work with the MSFR model, we assumed a pipe length of 2.255 m with salt flowing at 1.1275 m s^{-1} for an average out-of-core residence time of 2 seconds to follow the design specifications.

Neutronics Model

Since this region is largely subcritical, the only significant neutronics-related phenomena are the drift and decay of DNPs. The governing equation for the DNPs is:

$$\frac{\partial C_i}{\partial t} = -\lambda_i C_i - u\frac{\partial C_i}{\partial x} + D_t \frac{\partial^2 C_i}{\partial x^2}. \tag{3.10}$$

Equation 3.10 is derived from equation 3.2 by removing the fission DNP source term, and the conversion of the advection and diffusion terms to their 1-D forms. The decay constants and

diffusion coefficient are the same values used in the central core region.

Thermal-Hydraulics Model

Instead of the Navier-Stokes equations, we have a predetermined velocity of 1.1275 m s^{-1} in the outer loop region. The governing equation for temperature, derived from equation 3.7, is:

$$\rho c_p \frac{\partial T}{\partial t} = -\rho c_p u \frac{\partial T}{\partial x} - Q_{hx} \tag{3.11}$$

$$Q_{hx} = \alpha(T - T_s)\delta(x_0) \tag{3.12}$$

where

$$\alpha = \text{heat transfer coefficient [W K}^{-1}\text{]},$$

$$x_0 = \text{position of the point heat exchanger [m]}.$$

The fission heat source term is replaced with a heat exchanger sink term which depends on the temperature difference between the fuel salt T and the secondary loop salt T_s. For simplicity, we assumed a constant temperature of 823 K in the secondary loop. The heat transfer coefficient was determined by assuming that the fuel outlet temperature is 1023 K and calculating the heat removal rate to induce a 100 K drop at the given volumetric flow rate and heat capacity of the fuel salt. We opted to ignore the diffusion term due to the discontinuity of the temperature distribution across the point heat exchanger.

3.2.3 Boundary Conditions and Flow Transfers

This subsection details the various boundary conditions for all of the tracked variables, and the DNP and temperature flow transfers between the central core and outer loop regions.

Starting with the central core region, for the neutron group fluxes, we imposed vacuum boundary conditions on the outermost boundaries of the geometry in Figure 3.1 excluding the

axial boundary. The DNP variables have homogeneous Neumann boundary conditions along the axis and the walls in the central core region, and inflow and outflow boundary conditions on the inlet and outlet boundaries, respectively. The temperature variable shares the same type of boundary conditions as the DNP variables.

The flow rate is dictated by an inflow boundary condition at the core inlet for a volumetric flow rate of 4.5 m^3 s^{-1}. We imposed no-slip boundary conditions on the walls of the central core, and homogeneous Neumann boundary conditions on the outlet. Along the axial boundary, we have homogeneous Dirichlet boundary condition for the radial velocity component, and homogeneous Neumann boundary condition for the axial velocity component.

At every timestep, Moltres also calculates weighted averages of the temperature and DNP at the outlet. These values are weighted by the outflow velocity values at the outlet according to the following equation:

$$\overline{\phi} = \frac{\int_{\mathscr{C}} \phi(y)\,u(y)\,dy}{\int_{\mathscr{C}} u(y)\,dy} \qquad (3.13)$$

where

ϕ = variable to be weighted

$\mathscr{C}$ = outlet boundary curve

u = outflow velocity perpendicular to the outlet boundary [m s^{-1}].

This outflow value from the central core region is transferred to the 1-D outer loop region as input for the inhomogeneous Dirichlet boundary condition at the inlet boundary. Likewise, the outflow value from the outer loop region is used for the inflow value in the central core region. No averaging is required for this step as the outer loop region is a 1-D system. We assume that the inflow temperature and DNP are uniform at the inlet. The Picard iterations within every timestep ensure that the two systems are implicitly coupled even though they're solved separately.

Chapter 4

Neutronics Assessment

In this chapter, we compare key neutronics results between Serpent2 and Moltres for a static model of the MSFR, i.e. no salt flow, and uniform temperature distribution to assess the accuracy of the six-group neutron diffusion model in Moltres on a fast-spectrum reactor. This exercise also serves as a verification for the group constant data generated for Moltres from Serpent2.

4.1 Effective Multiplication Factor and Delayed Neutron Fraction

We calculated estimates of k_{eff} values in Serpent2 and Moltres for the MSFR model with static salt (no flow), and uniform temperature distributions. Moltres solves the six-group neutron diffusion equations as a steady-state eigenvalue problem to find the k_{eff} ~~as it does not currently have the capability to calculate the adjoint flux~~. Table 4.1 shows the k_{eff} values from Serpent2 and Moltres at 973 K and the corresponding salt density, while Table 4.1 shows the k_{eff} values for other temperatures at 100 K intervals. We observe small discrepancies on the order of 100 pcm between the two codes which we attribute to two main factors: the accuracy of the neutron diffusion model, and the omission of the blanket tank structural material. The neutron diffusion model is not as accurate as the other S_N or SP_N deterministic methods nor the Monte Carlo approach in Serpent2. Regarding the omission of the blanket tank material, we replaced the 2 cm-thick structural material with blanket salt. This replacement may be partly responsible for the higher k_{eff} value calculated by Moltres as the macroscopic fission cross sections of the

32

blanket salt are non-zero for the higher neutron energy groups. Nevertheless, the discrepancy is smaller than the 228.5 pcm and 256.7 pcm discrepancies reported by Cervi et al. [30] for their six-group SP_3 and neutron diffusion methods, respectively, in OpenFOAM. The neutron diffusion model in OpenFOAM is the same approach Aufiero et al. [7] used for their transient analysis of the MSFR, albeit with one neutron energy group.

Table 4.1: k_{eff} values from Serpent and Moltres at 973 K.

Code	k_{eff}	Difference wrt Serpent [pcm]
Serpent	1.00662(5)	-
Moltres with DNPs	1.0079488(10)	133
Moltres without DNPs	1.0049369(10)	-

[handwritten: are these zero or uncalculated?]

Table 4.2: k_{eff} values from Serpent and Moltres at various temperatures from 800 K to 1400 K.

Temperature [K]	$k_{eff} \pm 1\text{-}\sigma$ uncertainty (Serpent)	k_{eff} (Moltres)	Difference wrt Serpent [pcm]
800	1.01996(5)	1.02117	121
900	1.01172(5)	1.01322	150
1000	1.00428(5)	1.00544	116
1100	0.99735(5)	0.99859	124
1200	0.99006(5)	0.99119	113
1300	0.98356(5)	0.98439	83
1400	0.97702(5)	0.97820	118

[handwritten: do you mean $\pm\sigma$? k_{eff}]

The absolute value of k_{eff} largely impacts the steady-state temperature of the reactor. We may adjust k_{eff} by controlling fissile inventory to raise or lower the operating temperatures and meet the design specifications for inlet and outlet temperatures. For transient analysis, the β_{eff} and reactivity coefficients are arguably more important as they dictate the duration and magnitude of the reactor response to a transient initiator. The β_{eff} values at 973 K, shown in Table 4.3, are in excellent agreement with a 2.89 pcm discrepancy.

[handwritten: transient]

[handwritten: Flux does, yes. k_{eff} does not. Reactors have $k_{eff} \approx 1$ across all T.]

Table 4.3: β_{eff} values from Serpent and Moltres at 973 K.

Code	β_{eff} [pcm]	Difference wrt Serpent [pcm]
Serpent	304.08(81)	-
Moltres	301.19(20)	2.89

4.2 Reactivity Feedback Coefficients

The temperature reactivity feedback arises mainly from Doppler broadening of resonance absorption peaks and temperature-induced density changes. Although Doppler coefficients typically show logarithmic dependence to temperature, we report them, along with the other coefficients, as linear gradient values of the reactivity given the relatively linear trend within the relevant temperature range (Figure 4.1). Table 4.4 shows the temperature coefficients as described prior. The total temperature coefficients from Serpent and Moltres show excellent agreement with a discrepancy of 0.019 pcm K^{-1}.

[Handwritten annotation: You didn't though. Your plot doesn't make a linear regression. It just connects the dots, piecewise.]

[Handwritten annotation: Phase change (melting point of the LiF salt.)]

Figure 4.1: Reactivity values from Serpent and Moltres. The Doppler reactivity values were calculated at a fixed density of 4.1249 g cm^{-3}. The density reactivity values were calculated at a fixed temperature of 973 K.

Table 4.4: Doppler, density, and total temperature coefficients for the temperature range of 800 K to 1400 K.

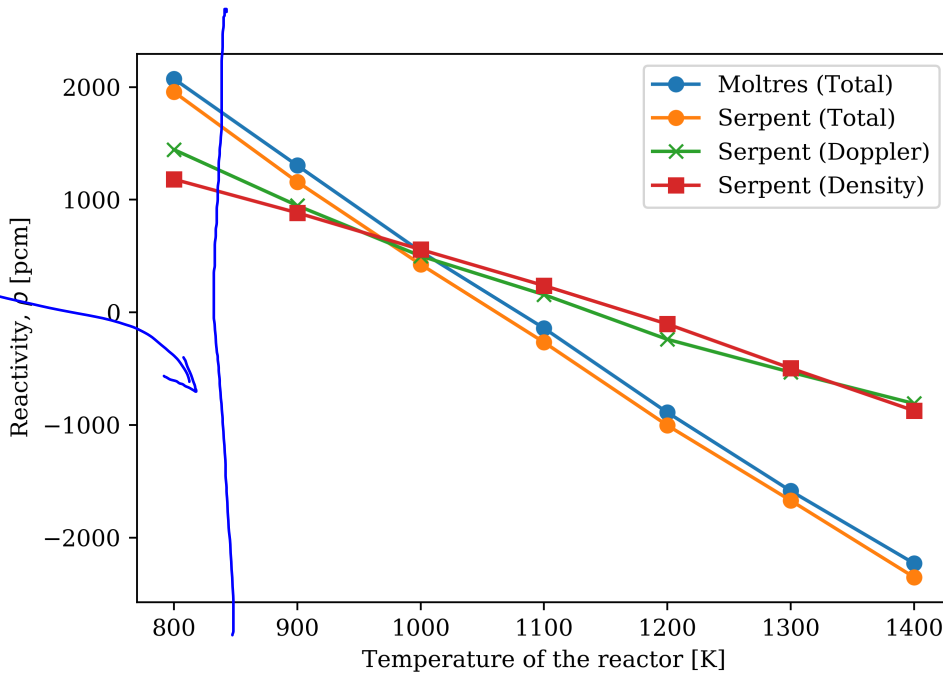| Code	α_D (log) [pcm]	α_D (linear) [pcm K^{-1}]	α_ρ [pcm K^{-1}]	α_T [pcm K^{-1}]
Serpent	−4034(14)	3.737(13)	3.424(13)	7.165(13)
Moltres	-	-	-	7.184

4.3 Neutron Energy Spectrum
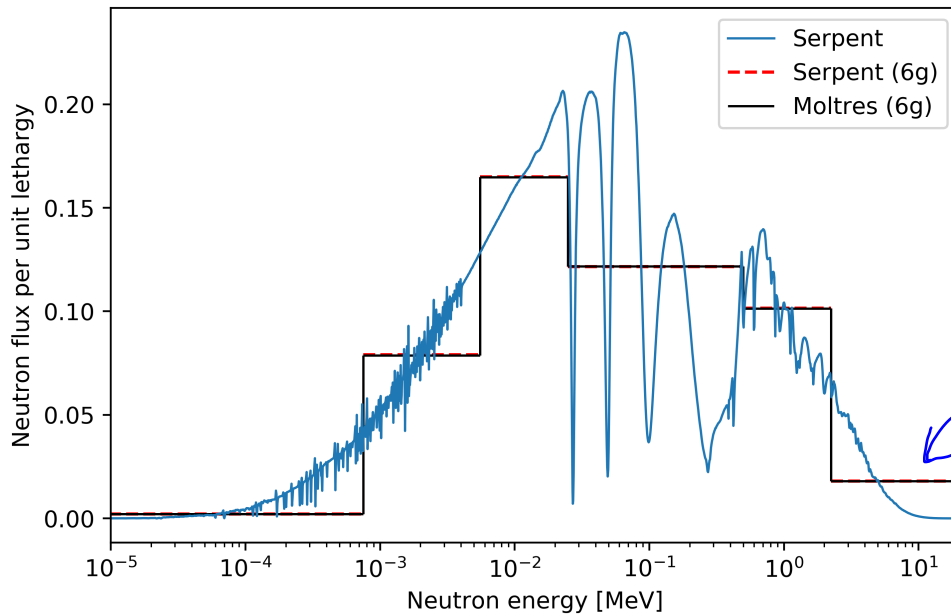
Figure 4.2: Reactivity values from Serpent and Moltres. The Doppler reactivity values were calculated at a fixed density of 4.1249 g cm^{-3}. The density reactivity values were calculated at a fixed temperature of 973 K.

Moltres also reproduced the six-group neutron spectrum very well from the Serpent group constants. Figure 4.2 compares the energy spectra from Serpent and Moltres in the central fuel salt region. The six-group neutron spectra overlap exactly over each other. More generally, the plot shows the distinctive fast spectrum observed in the MSFR with dips in the spectrum corresponding to elastic scattering resonances from lithium and fluorine. From this plot, we observe that the discrepancies in k_{eff} arise mainly from discretizing neutron energy into groups rather than the neutron diffusion model itself. We could obtain a more accurate representation

of the neutronics in the MSFR by using more neutron energy groups but this would adversely impact simulation times in the subsequent multiphysics finite element analyses.

In summary, Moltres can replicate most of the relevant neutronics parameters accurately with the group constant data from Serpent. While the k_{eff} values have discrepancies on the order of 100 pcm, they are relatively small compared to results from other codes. Furthermore, the β_{eff} and temperature coefficients, which are important parameters for modeling transient reactor behavior, are in excellent agreement.

[handwritten annotation: If this sentence were not in passive voice, it would be clear that the agreement is "Moltres agrees with the high fidelity simulation in Serpent"]

[handwritten annotation: "effective delayed neutron fraction, β_{eff}"]

References

[1] IEA, "Global Energy and CO2 Status Report 2018," tech. rep., International Energy Agency, Paris, France, Mar. 2019.

[2] GIF, "A technology roadmap for generation IV nuclear energy systems," Tech. Rep. GIF-002-00, US DOE Nuclear Energy Research Advisory Committee and the Generation IV International Forum, 2002.

[3] J. Krepel, U. Rohde, U. Grundmann, and F.-P. Weiss, "DYN3D-MSR spatial dynamics code for molten salt reactors," *Annals of Nuclear Energy*, vol. 34, pp. 449–462, June 2007.

[4] J. Kophazi, D. Lathouwers, and J. Kloosterman, "Development of a Three-Dimensional Time-Dependent Calculation Scheme for Molten Salt Reactors and Validation of the Measurement Data of the Molten Salt Reactor Experiment," *Nuclear Science and Engineering*, vol. 163, no. 2, pp. 118–131, 2009.

[5] A. Cammi, V. Di Marcello, L. Luzzi, V. Memoli, and M. E. Ricotti, "A multi-physics modelling approach to the dynamics of Molten Salt Reactors," *Annals of Nuclear Energy*, vol. 38, pp. 1356–1372, June 2011.

[6] C. Fiorina, D. Lathouwers, M. Aufiero, A. Cammi, C. Guerrieri, J. L. Kloosterman, L. Luzzi, and M. E. Ricotti, "Modelling and analysis of the MSFR transient behaviour," *Annals of Nuclear Energy*, vol. 64, pp. 485–498, Feb. 2014.

[7] M. Aufiero, A. Cammi, O. Geoffroy, M. Losa, L. Luzzi, M. E. Ricotti, and H. Rouch, "Development of an OpenFOAM model for the Molten Salt Fast Reactor transient analysis," *Chemical Engineering Science*, vol. 111, pp. 390–401, May 2014.

[8] M. Zanetti, A. Cammi, C. Fiorina, and L. Luzzi, "A Geometric Multiscale modelling approach to the analysis of MSR plant dynamics," *Progress in Nuclear Energy*, vol. 83, pp. 82–98, Aug. 2015.

[9] A. Laureau, D. Heuer, E. Merle-Lucotte, P. R. Rubiolo, M. Allibert, and M. Aufiero, "Transient coupled calculations of the Molten Salt Fast Reactor using the Transient Fission Matrix approach," *Nuclear Engineering and Design*, vol. 316, pp. 112–124, May 2017.

[10] M. W. Rosenthal, P. R. Kasten, and R. B. Briggs, "Molten-Salt Reactors - History, Status, and Potential," *Nuclear Applications and Technology*, vol. 8, pp. 107–117, Feb. 1970.

[11] P. N. Haubenreich and J. R. Engel, "Experience with the Molten-Salt Reactor Experiment," *Nuclear Technology*, vol. 8, pp. 118–136, Feb. 1970.

[12] H. G. MacPherson, "The Molten Salt Reactor Adventure," *Nuclear Science and Engineering*, vol. 90, pp. 374–380, Aug. 1985.

[13] J. C. Gehin and J. J. Powers, "Liquid Fuel Molten Salt Reactors for Thorium Utilization," *Nuclear Technology*, vol. 194, pp. 152–161, May 2016.

[14] J. Smith and W. E. Simmons, "An assessment of a 2500 MWe molten chloride salt fast reactor," Tech. Rep. AEEW-R956, United Kindom Atomic Energy Authority, Aug. 1974.

[15] A. Rykhlevskii, J. W. Bae, and K. D. Huff, "Modeling and simulation of online reprocessing in the thorium-fueled molten salt breeder reactor," *Annals of Nuclear Energy*, vol. 128, pp. 366–379, June 2019.

[16] B. M. Elsheikh, "Safety assessment of molten salt reactors in comparison with light water reactors," *Journal of Radiation Research and Applied Sciences*, vol. 6, pp. 63–70, Oct. 2013.

[17] I. K. Aji, T. Tatsuya, M. Kinoshita, and T. Okawa, "An Experimental and Numerical Study of Wall Effect on Freeze Valve Performance in a Molten Salt Reactor," *Journal of Nuclear Engineering and Radiation Science*, vol. 6, Apr. 2020.

[18] M. Brovchenko, D. Heuer, E. Merle, M. Allibert, V. Ghetta, A. Laureau, and P. Rubiolo, "Design-Related Studies for the Preliminary Safety Assessment of the Molten Salt Fast Reactor," *Nuclear Science and Engineering*, vol. 175, pp. 329–339, Nov. 2013.

[19] L. Mathieu, D. Heuer, R. Brissot, C. Garzenne, C. Le Brun, D. Lecarpentier, E. Liatard, J.-M. Loiseaux, O. Mãľplan, E. Merle-Lucotte, A. Nuttin, E. Walle, and J. Wilson, "The thorium molten salt reactor: Moving on from the MSBR," *Progress in Nuclear Energy*, vol. 48, pp. 664–679, Sept. 2006.

[20] J. Serp, M. Allibert, O. Benes, S. Delpech, O. Feynberg, V. Ghetta, D. Heuer, D. Holcomb, V. Ignatiev, J. L. Kloosterman, L. Luzzi, E. Merle-Lucotte, J. UhlÃɳÅŹ, R. Yoshioka, and D. Zhimin, "The molten salt reactor (MSR) in generation IV: Overview and perspectives," *Progress in Nuclear Energy*, vol. 77, pp. 308–319, Nov. 2014.

[21] M. Brovchenko, J.-L. Kloosterman, L. Luzzi, E. Merle, D. Heuer, A. Laureau, O. Feynberg, V. Ignatiev, M. Aufiero, A. Cammi, C. Fiorina, F. Alcaro, S. Dulla, P. Ravetto, L. Frima, D. Lathouwers, and B. Merk, "Neutronic benchmark of the molten salt fast reactor in the frame of the EVOL and MARS collaborative projects," *EPJ Nuclear Sciences & Technologies*, vol. 5, p. 2, Jan. 2019.

[22] S. Delpech, E. Merle, D. Heuer, M. Allibert, V. Ghetta, C. Le-Brun, X. Doligez, and G. Picard, "Reactor physic and reprocessing scheme for innovative molten salt reactor system," *Journal of Fluorine Chemistry - J FLUORINE CHEM*, vol. 130, Jan. 2009.

[23] J. Leppanen, M. Pusa, T. Viitanen, V. Valtavirta, and T. Kaltiaisenaho, "The Serpent Monte Carlo code: Status, development and applications in 2013," *Annals of Nuclear Energy*, vol. 82, pp. 142–150, Aug. 2014.

[24] OECD/NEA, "The JEFF-3.1.2 Nuclear Data Library," Tech. Rep. JEFF Report 24, OECD/NEA Data Bank, OECD/NEA, 2014.

[25] D. R. Gaston, C. J. Permann, J. W. Peterson, A. E. Slaughter, D. AndrÅą, Y. Wang, M. P. Short, D. M. Perez, M. R. Tonks, J. Ortensi, L. Zou, and R. C. Martineau, "Physics-based multiscale coupling for full core nuclear reactor simulation," *Annals of Nuclear Energy*, vol. 84, pp. 45–54, Oct. 2015.

[26] B. S. Kirk, J. W. Peterson, R. H. Stogner, and G. F. Carey, "libMesh: a C++ library for parallel adaptive mesh refinement/coarsening simulations," *Engineering with Computers*, vol. 22, pp. 237–254, Dec. 2006.

[27] B. Satish, A. Shrirang, M. F. Adams, J. Brown, P. Brune, K. Buschelman, L. Dalcin, A. Dener, V. Eijkhout, W. D. Gropp, D. Karpeyev, D. Kaushik, M. G. Knepley, D. A. May, L. C. McInnes, R. T. Mills, T. Munson, K. Rupp, P. Sanan, B. F. Smith, S. Zampini, and H. Zhang, "PETSc Users Manual," Tech. Rep. ANL-95/11 - Revision 3.12, Argonne National Laboratory, 2019.

[28] M. Aufiero, A. Cammi, C. Fiorina, J. LeppÃd'nen, L. Luzzi, and M. E. Ricotti, "An extended version of the SERPENT-2 code to investigate fuel burn-up and core material evolution of the Molten Salt Fast Reactor," *Journal of Nuclear Materials*, vol. 441, pp. 473–486, Oct. 2013.

[29] J. W. Peterson, A. D. Lindsay, and F. Kong, "Overview of the Incompressible Navier-Stokes simulation capabilities in the MOOSE Framework," *arXiv:1710.08898 [math]*, Oct. 2017. arXiv: 1710.08898.

[30] E. Cervi, S. Lorenzi, A. Cammi, and L. Luzzi, "Development of an SP3 neutron transport solver for the analysis of the Molten Salt Fast Reactor," *Nuclear Engineering and Design*, vol. 346, pp. 209–219, May 2019.